Supporting Information for

Charge Transfer Dynamics Between Photoexcited CdS Nanorods and Mononuclear Ru Water-Oxidation Catalysts

Huan-Wei Tseng,[‡] Molly B. Wilker,[‡] Niels H. Damrauer,* and Gordana Dukovic*

Department of Chemistry and Biochemistry, University of Colorado Boulder,
Boulder, Colorado 80309, United States

[‡] These authors contributed equally to this work.

* Corresponding Authors: Gordana.Dukovic@colorado.edu; Niels.Damrauer@colorado.edu

Table of Contents

1. Experimental details

Synthesis of CdS Nanorods. The CdS nanorods were synthesized using a previously reported procedure.[1-3] Synthesis and processing were performed under an inert argon atmosphere at ~620 Torr (the atmospheric pressure in Boulder, CO). 8.54 mmol trioctylphosphine oxide (TOPO; Sigma Aldrich, *ReagentPlus*®, 99%), 3.2 mmol n-octadecylphosphonic acid (ODPA; PCI Synthesis), 1.61 mmol cadmium oxide (CdO; Sigma Aldrich, ≥99.99% trace metals basis) were stirred under vacuum at 120ºC and then heated under Ar to 320ºC for 1hr. The mixture was then cooled to 120ºC, stirred under vacuum for 1h, and then heated again under Ar to 320ºC. 5.40 mmol tri-n-octylphosphine (TOP; Strem Chemicals, min. 97%), and 3.2 mmol trioctylphosphine sulfide (TOP:S) were injected. TOP:S was prepared by mixing TOP and elemental S (Aldrich, 99.998%) in a 1:1 molar ratio in an argon glovebox and stirring at room temperature for 48 hours. After TOP:S injection, nanocrystal growth proceeded at 315ºC for 45 minutes. The reaction mixture was then cooled to 80ºC, and the nanocrystals were precipitated using a toluene:acetone (1:2 volume ratio) mixture. The CdS nanocrystals were purified under Ar through sequential re-dispersion/precipitation steps using toluene/octylamine/acetone, chloroform/nonanoic acid/isopropanol, and hexane/isopropanol mixtures. Finally, sequential precipitation steps using increasing amounts of isopropanol were used to separate the mixture into fractions with narrower length distribution. The purified nanocrystals were re-dispered and stored in toluene.

The resulting highly monodisperse nanorods had an average diameter of 4.0 ± 0.4 nm and an average length of 13.7 ± 2.3 nm (one standard deviation for both dimensions), as determined by measurements of over 200 particles in TEM images. The molar absorptivity (ε) of the CdS nanorods was determined by correlating absorption spectra with Cd^{2+} concentrations determined by elemental analysis (ICP-OES) of acid-digested samples. The estimated value of $\varepsilon_{350\ nm}$ was 1710 $M^{-1}cm^{-1}$ per Cd^{2+}. The number of Cd^{2+} per nanorod was estimated from average nanorod dimensions. $\varepsilon_{350\ nm}$ for this batch of nanorods was 6 x 10^6 $M^{-1}cm^{-1}$.

For solvent compatibility with complex **1**, the hydrophobic surface-capping ligands were replaced with 3-mercaptopropionic acid (3-MPA) under Ar following a previously reported procedure.[1] First, a 70 mM solution of 3-mercaptopropionic acid (3-MPA;Sigma Aldrich ≥99%) in methanol was prepared. The pH of the 3-MPA solution was raised to pH 11 with tetramethylammonium hydroxide pentahydrate (Sigma ≥97%). Next, a sample of the original, organic-capped, nanocrystals in toluene was precipitated using methanol. The precipitated nanocrystals were then vigorously mixed with the 70 mM 3-MPA solution until no longer cloudy. A large amount of toluene was added to the solution to precipitate the 3-MPA-capped nanocrystals. The resulting particles were collected and then re-dissolved in HPLC-grade MeOH.

Transmission Electron Microscopy (TEM). TEM samples were prepared by drop casting from solution onto carbon film, 300 mesh, copper grids from Electron Microscopy Sciences. Images were obtained using a 100KV Phillips CM100 TEM equipped with a bottom-mounted 4 megapixal AMT v600 digital camera. Nanorod dimensions were obtained using *ImageJ* software to measure more than 200 nanocrystals.

Synthesis of Ru(II) Complexes. [Ru(dcb)(tpy)Cl]Cl and [Ru(deeb)(tpy)Cl](PF_6) (Complex **1)** were synthesized according to published procedures.[4,5] [Ru(dcb)(tpy)Cl]Cl was dissolved in H_2O and precipitated by adding $HPF_{6(aq)}$ to afford [Ru(dcb)(tpy)Cl](PF_6). ESI(+) MS and ^{1}H-NMR

chemical shifts matched the published values.[4,5] ESI(+) MS and ^{1}H-NMR characterization of **1** in MeOH did not reveal evidence of Cl ligand displacement by the solvent.

Coupling of CdS NR to Complex 1. To form the CdS-**1** hybrid system, HPLC grade MeOH (Sigma-Aldrich) solutions of CdS NRs and **1** were mixed, and samples sealed under Ar. Absorption spectra were recorded in 1 cm path length quartz cuvettes at room temperature with an Agilent 8453 spectrophotometer equipped with tungsten and deuterium lamps. The concentration of **1** in each solution was determined from the absorbance at 520 nm (ε = 16000 M^{-1} cm^{-1} measured in MeOH) where there is no contribution from the NRs. The CdS NR concentration was determined from the absorbance at 350 nm following subtraction of the absorbance from **1**. For samples associated with Figure 3c, methanol solutions of ascorbate (derived from ascorbic acid (Sigma-Aldrich BioXtra, ≥ 99.0%) using tetramethylammonium hydroxide pentahydrate (Sigma ≥ 97%) to raise the pH) or methylene blue (MB) hydrate (Aldrich) were added. The ascorbate solution was 1.6 x 10^{-4} M and was combined with the nanocrystals in a 1:1700 (CdS NR: ascorbate) ratio. The MB solution was 3.5 mM and was combined in a 1:200 (CdS NR:MB) ratio.

Photoluminescence Spectra. Photoluminescence spectra were obtained at room temperature using a PTI fluorometer with an Ushio UXL-75XE xenon short arc lamp and a Hamamatsu R928P PMT tube operating at −1000 V, DC. Samples in 1 cm x 1 cm quartz cuvettes were excited at 360 nm and the emission from 425 nm to 700 nm was recorded at 90° relative to the excitation. Emission spectra were corrected for wavelength dependence of the instrument response. A detailed description of the instrumentation was published previously.[6] CdS NR concentration was 0.18 μM.

Ultrafast Transient Absorption (TA) Spectroscopy: The ultrafast (100 fs to 3.3 ns) TA spectrometer used in this study uses an amplified Ti:sapphire laser (Solstice, Spectra-Physics, 800 nm, 1 kHz, 100 fs, 3.5 mJ/pulse), an optical parametric amplifier (TOPAS-C, Light Conversion), and the Helios spectrometer (Ultrafast Systems, LLC). A fraction (1.6 mJ/pulse) of the 800nm Solstice output was directed to the TOPAS-C to produce the desired pump wavelength (400 nm in the data described here) for sample excitation, which was then directed into the Helios. The pump pulse beam waist (~350 μm) and energy (<10 nJ/pulse) were chosen to maintain a nanocrystal excitation probability below 0.3 per laser pulse to avoid excitation of multiple electron-hole pairs within the nanocrystals. The pump pulses were passed through a depolarizer and chopped by a synchronized chopper to 500 Hz before reaching the sample. Another fraction of the 800 nm Solstice output (~0.1 mJ/pulse) was guided directly into the Helios for generation of the probe. Within the spectrometer, a white light continuum of wavelengths including 450 – 800 nm was generated using a sapphire plate. This beam was split into a probe and a reference beam. The probe beam was focused into the sample where it was overlapped with the pump beam. The transmitted probe and reference beams were then focused into optical fibers coupled to multichannel spectrometers with CMOS sensors with 1 kHz detection rates. The reference signal is used to correct the probe signal for pulse-to-pulse fluctuations in the white-light continuum. The time delay between the pump and probe pulses was controlled by a motorized delay stage. For all transient absorption measurements, the sample was sealed under Ar in a 2 mm quartz cuvette equipped with a Kontes valve and constantly stirred. CdS NR concentrations were approximately 0.8 μM. All experiments were conducted at

room temperature. The change in absorbance signal (ΔA) was calculated from the intensities of sequential probe pulses with and without the pump pulse excitation. The data collection (500 pump shots per time point) was carried out three consecutive times to ensure no photo-induced changes occurred. The three traces were then averaged.

Nanosecond-Microsecond Transient Absorption Spectroscopy: The 0.3 ns – 400 μs TA spectrometer used the amplified Ti:sapphire laser and optical parametric amplifier described above coupled with the Eos spectrometer (Ultrafast Systems, LLC). The pump beam (400 nm) was depolarized and the power was controlled with neutral density filters. The pump-probe time delay was controlled by a digital delay generator (CNT-90, Pendulum Instruments). The white light continuum (400 – 900 nm) for the probe and reference beams was generated by an external 2 kHz Nd:YAG laser focused into a photonic crystal fiber. The probe and reference signals were focused into the same detectors as used for the ultrafast TA system. Helios and Eos ΔA kinetic traces were combined using *Surface Xplorer Pro* by Ultrafast Systems, LLC.

2. Construction of energy level diagram in Fig. 1d

The band edges of CdS NRs, which are quantum confined in the radial direction, were approximated using the Brus equation.[7] The bulk band gap energy (2.5 eV) and the valence band position with respect to vacuum (-6.26 eV) were obtained from Ref 8.[8] The quantum confined band gap was determined from the steady state band edge absorption edge (2.64 eV), and the valence and conduction band edges were adjusted taking into account the effective masses of the electron (0.2 m_0) and the hole (0.7 m_0).[9] The vacuum scale was then converted to NHE (-4.4 eV (vacuum) ≈ 0 V NHE). The one-electron oxidation and reduction potentials of **1** in MeCN have been previously reported.[4,10] Although the system is studied in MeOH for this paper, no further modifications to the redox potentials are made because solvent-based redox potential changes have been observed to be small for a large and coordinatively-saturated complex such as **1**.[11] The first oxidation potential ($Ru^{3+/2+}$) of **1** is 0.7 V less positive than the NR VB edge, which should then permit hole-transfer to **1** following photoexcitation of the NR. Conversely, the CB edge of the NR is 0.2 V more positive than the 2+/1+ couple of **1,** which should hinder photoinduced electron transfer from the NR to the LUMO of the catalyst.

3. CdS NR photoluminescence in the presence of complex 1 and free ligands

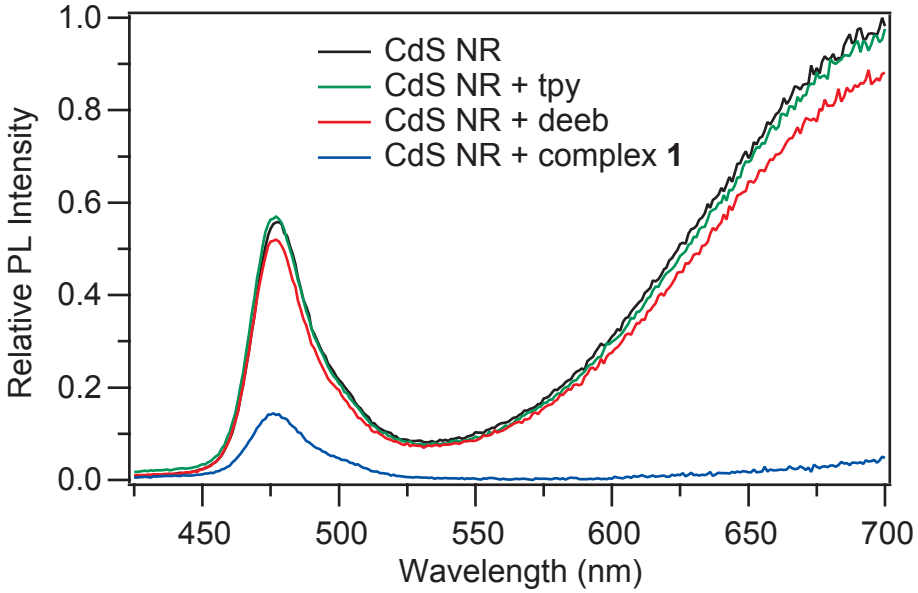

Figure S1. PL spectra recorded in MeOH for CdS NR (black trace) and CdS NR with free ligands tpy (green trace), deeb (red trace), or with complex **1** (blue trace). The ratios of CdS NR to quenchers are all 1 to 50. The PL of CdS NR is significantly quenched by **1**, but not by tpy or deeb. This suggests that the Ru center of the complex is required for PL quenching.

4. Differentiating Stern-Volmer and Langmuir models for CdS NR interaction with complex 1

To elucidate the interaction between the CdS NRs and complex **1**, we analyzed the quenching of CdS NR PL by **1** (Figure 2). We considered two models: a Stern-Volmer model for dynamic quenching via collisions and a Langmuir model for static quenching due to adsorbed quenchers.

For pure collisional quenching in a homogeneous solution, a plot of I_0/I_Q vs [Q] should follow the linear form of the Stern-Volmer equation:

$$\frac{I_0}{I_Q} = 1 + K_{SV}[Q] \qquad \text{Eq. S1}$$

where I_0 is the PL intensity of CdS NR without quencher, I_Q is the PL intensity of CdS NR with quencher, K_{SV} is the Stern-Volmer constant, and [Q] is the concentration of quencher. The band gap and trap emission quenching (I_0/I_Q) vs [Q] are shown in Figures S2a and b. The data for the band gap transition are clearly a poor fit to Eq. S1. The quenching of the trap emission fits the Stern-Volmer model better. However, we note that the trap emission was significantly weaker than band gap emission at increased **1**:CdS NR ratios (Figure 2) and thus there is higher uncertainty in the data in Figure S2b. Furthermore, because trap states are longer lived than band gap states, they may be more susceptible to collisional quenching. Overall, given the poor fit of the quenching of the band gap transition to the Stern-Volmer model, we conclude that collisions alone cannot account for the concentration-dependent quenching of CdS PL.

Next, we consider the Langmuir adsorption model for the CdS-**1** interaction. Assuming that quenching is caused by adsorption of molecules, we can write the Langmuir adsorption isotherm as:

$$\theta = \frac{K \cdot [Q]}{1 + K \cdot [Q]} \qquad \text{Eq. S2}$$

where Q is quencher (the adsorbate), θ is the fraction of surface sites occupied by the quencher, and K is the equilibrium constant for adsorption of **1** on CdS surface. We assume that θ is equal to the fraction of PL quenched ($\Delta I/I_0$). Here, I_0 is the PL intensity of CdS NR with no quencher present, while ΔI ($=I_0-I_Q$) is the amount of PL quenched in the presence of quencher. An additional complication is that, unlike trap emission, band gap emission was not fully quenched at saturation. We attribute this to a lower quenching efficiency for the band-gap emission caused by its shorter lifetime compared to the trap emission.[12] To account for the incomplete quenching, we introduce the term, $(\Delta I/I_0)_{max}$, which is the maximum fractional quenching observed.[13] Eq. S2 then becomes:

$$\frac{\Delta I}{I_0} = \frac{(\Delta I/I_0)_{max} \cdot K \cdot [Q]}{1 + K \cdot [Q]} \qquad \text{Eq. S3}$$

Eq. S3 was used for the fit shown in Figure 2 within the manuscript. For a more direct comparison with the Stern-Volmer model, Eq. S3 can be rearranged to give the linear form:

$$\frac{I_0}{\Delta I} = \frac{1}{(\Delta I/I_0)_{max}} \cdot \frac{1}{K[Q]} + \frac{1}{(\Delta I/I_0)_{max}} \qquad \text{Eq. S4}$$

As shown in Figures S2c and d, the dependence of CdS PL quenching on concentration of **1** is fit well with Eq. S4. For the band gap transition, we find that $K = 9.5 \times 10^5\ M^{-1}$ and $(\Delta I/I_0)_{max} = 0.83$, whereas for the trap emission the parameters are $K = 1.6 \times 10^6\ M^{-1}$ and $(\Delta I/I_0)_{max} = 1.0$. Like the difference in the values of $(\Delta I/I_0)_{max}$ mentioned above, the difference in the values of K may be attributable to different quenching efficiencies for the two transitions. Given the same number of bound quenchers, more of the trap emission would be quenched, compared to band gap emission, resulting in a higher apparent value of K. Another way to state this is that K is actually a combination of an equilibrium constant and a quenching efficiency.

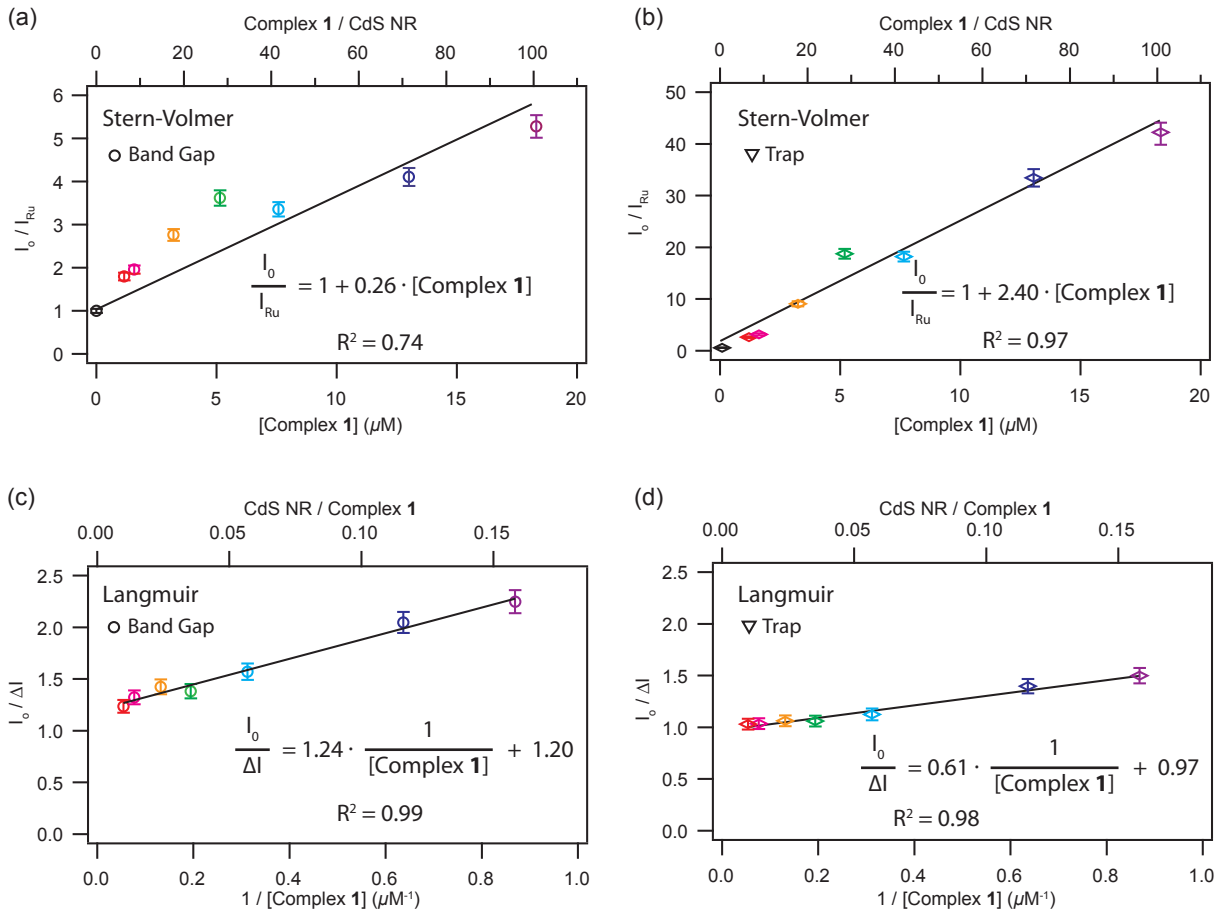

Figure S2. Quenching of CdS PL emission as a function of concentration of **1**. In (a) and (b), band gap and trap emission are fit with the Stern-Volmer model for dynamic collisional quenching, whereas in (c) and (d) the same data is fit with a linear form of the Langmuir adsorption isotherm. Error bars were determined by comparing three PL spectra taken over a period of 1 hour for one sample with a CdS:**1** ratio of 1:43 and one CdS-only sample. The error was then propagated in an additive fashion to obtain the total value of ± 5%. This method overestimates the uncertainty in the measurement.

5. Supporting information for transient absorption spectra and excited state decay kinetics

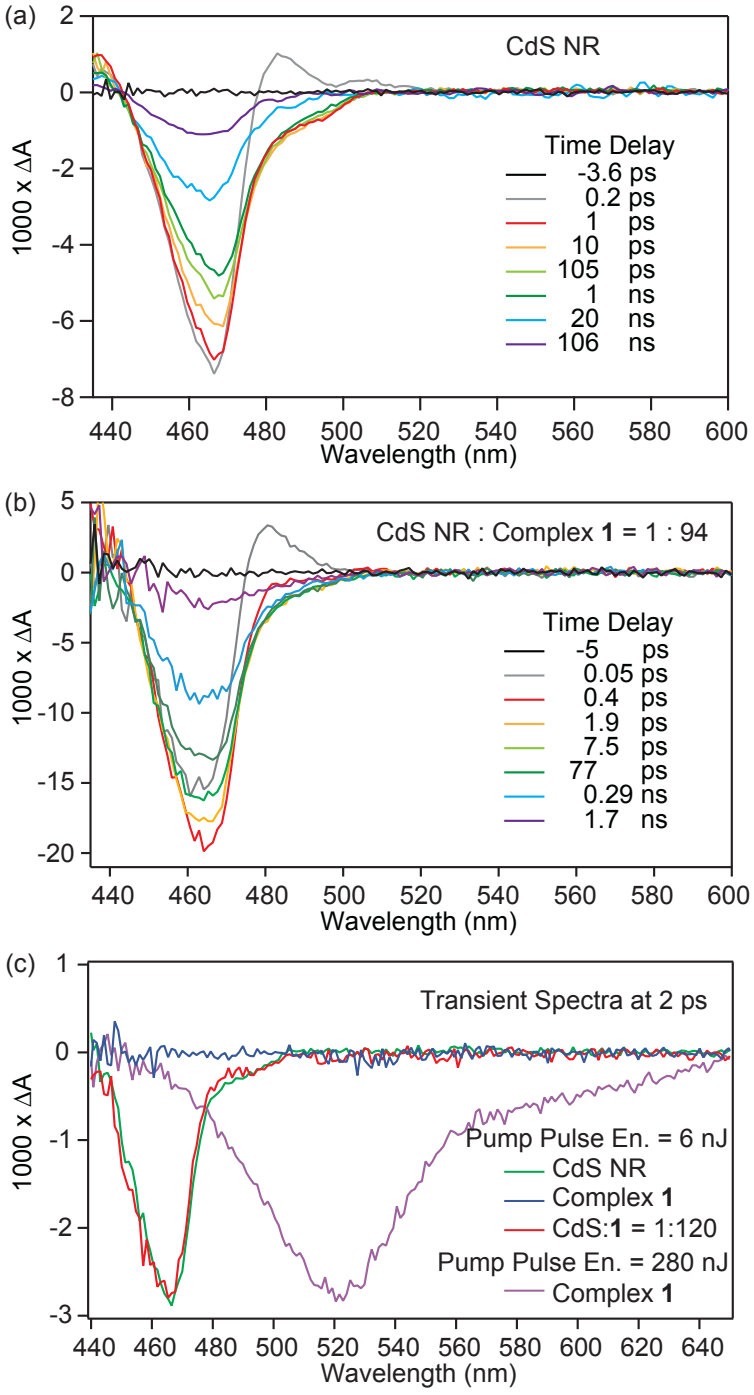

Figure S3. Transient absorption spectra of (a) CdS NRs in MeOH and (b) CdS with **1** in a 1 : 94 ratio at different time delays following 400 nm excitation. The strong CdS bandgap bleach feature appears around 470 nm. In addition, a rapidly decaying absorption feature is observed at 482 nm, red-shifted from the exciton bleach feature. This has been attributed to the bi-exciton shift due to hot excitons, and its decay corresponds to carrier cooling.[14] A second absorption

feature at higher-energy (~440 nm) corresponds to higher energy exciton bands.[14,15] The presence of **1** does not change the position or shape of the CdS spectral features nor are there additional features in the TA associated with **1**. Transient features of **1** are not observable because of the vast difference in molar absorptivities ($\varepsilon_{400\,nm}$ for CdS NR= 4 x 10^6 M^{-1} cm^{-1}; $\varepsilon_{400\,nm}$ for complex **1** = 1 x 10^4 M^{-1} cm^{-1}). (c) Transient absorption spectra of CdS NRs, CdS + **1** (1:120 molar mixture), and **1** taken 2 ps after excitation with a 400 nm pump. Under the normal conditions for the TA experiments (pump pulse energy 6 nJ), there is no transient signal observed from **1**. When the pulse energy is increased 47-fold to 280 nJ, a sample containing **1** only exhibits a bleach ~520 nm.

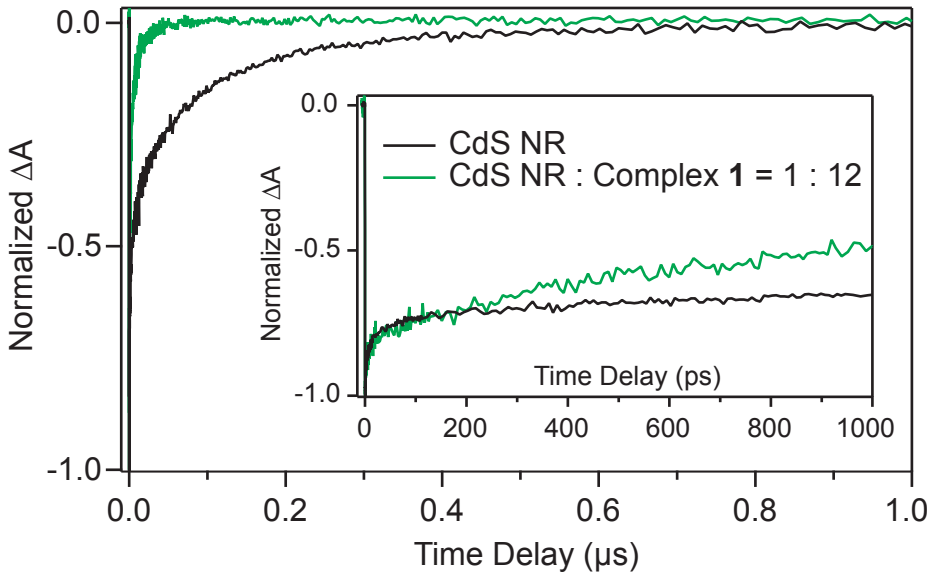

Figure S4. TA kinetics at 470 nm for CdS NRs in the presence and absence of complex **1** plotted with a linear time scale. Note that the excited state lifetime is considerably shortened with the addition of **1**. The inset plot of the first nanosecond of kinetics shows that the two samples have overlapping dynamics for the first 250 ps before diverging due to ET.

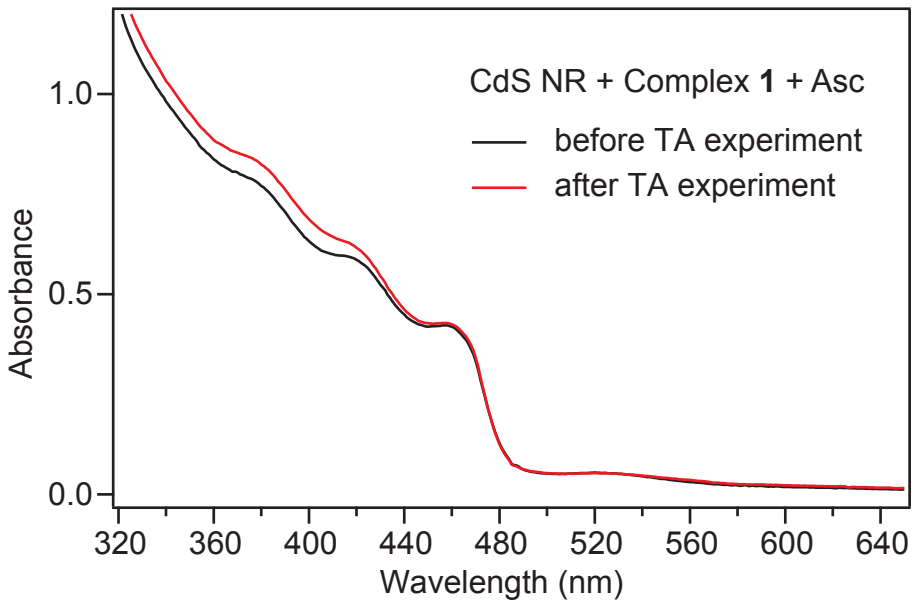

Figure S5. Steady-state absorption spectra of a sample containing CdS NRs, complex **1**, and ascorbate (Asc) taken before and after TA data collection. The difference in absorption around 380 nm can be attributed to an increase in the concentration of an oxidized form of ascorbate.[16]

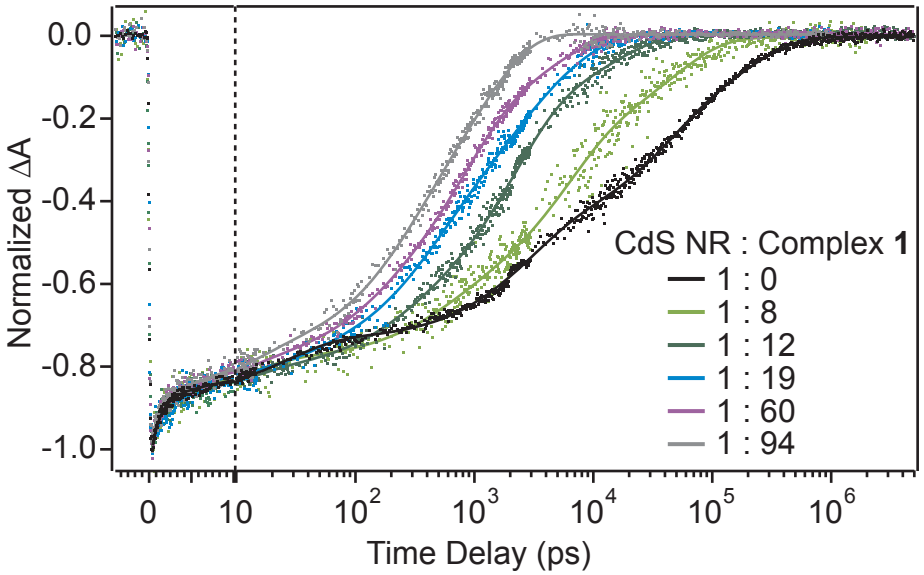

Figure S6. Transient absorption kinetics of CdS NRs with fixed concentration of CdS NRs and varying CdS NR:**1** ratios. The excited state lifetime shortens with increasing concentration of **1**. Solid lines are five-exponential fits to the data.

The TA kinetics in Figure S6 provide information about timescales of both the hole transfer (HT) and electron transfer (ET) events between CdS NRs and **1**. Within our model (Figure 3 and related discussion), HT from CdS valence band and hole traps to the HOMO of **1** is followed by ET from the CdS conduction band into the newly available empty state in **1**, resulting in overall electron-hole recombination at the metal center.

The point at which the CdS-**1** kinetics diverge from the CdS kinetics was defined as the onset of ET (HT must occur before an electron acceptor state becomes available). The determination of the point of divergence is somewhat subjective, but we can estimate it by the following method: with a logarithmic x-axis, for each complex **1**: CdS NR sample, the ns-range ET pathway was fit to a line. The intersection of this line with a line parallel to the 1 ps-1 ns portion of the CdS-only decay was estimated to be the ET onset time. The results are summarized in Table S1 and plotted in Figure S7a. Note that the ET onset times exhibit a saturation behavior similar to that shown by PL quenching (Figure 2).

Information about the dynamics of the ET that follows HT is provided by the kinetics of the bleach decay. Because the CdS band gap decay behavior is multi-exponential, we cannot form a meaningful physical model attributing each component to a specific process without additional information. Instead, we focus on values that are relatively insensitive to the number of fit parameters. The average excited state lifetimes were calculated as,[17]

$$< \tau_{measured} > = \frac{\sum_i a_i \tau_i^2}{\sum_i a_i \tau_i}, \qquad \text{Eq. S5}$$

where a_i and τ_i are the parameters from a multi-exponential fit. For CdS alone, we determined, by inspection of the residual, that the minimum number of exponentials needed for a good fit is five. The time-components obtained were at least one order of magnitude apart in time. For CdS-**1** samples, the fits to both four and five exponentials were suitable and they resulted in essentially identical values of $< \tau_{measured} >$ (Table S1).

Since ΔA is proportional to the electron population, integral of the decay signal is proportional to the total population over the decay time. We can calculate the quantum efficiency of electron transfer (QE_{ET}) from the integrated areas under the kinetic decays or their fitting curves using[17]

$$QE_{ET} = 1 - \frac{\int \Delta A(CdS+\mathbf{1})}{\int \Delta A(CdS)}. \qquad \text{Eq. S6}$$

Then we can estimate the average lifetime of ET ($< \tau_{ET} >$) by adapting the expression used for single-exponential excited state decays, $\tau_{ET} = \frac{\tau_{measured}}{QE_{ET}}$, as

$$< \tau_{ET} > \approx \frac{< \tau_{measured} >}{QE_{ET}}. \qquad \text{Eq. S7}$$

For consistency, we used $<\tau_{measured}>$ values from five-exponential fits, but essentially identical numbers are obtained from four-exponential fits for the CdS-**1** complexes. Eq. S7 likely underestimates τ_{ET} because longest-lived components likely have highest efficiencies of ET. Nevertheless, this treatment allows us to determine lower limits for ET lifetimes. The results of this analysis are summarized in Table S1 and plotted in Fig S7b.

We expected the HT and ET processes to have similar dependencies on the concentration of **1** because the fraction of photoexcited CdS NRs that undergo ET is governed by the fraction that first undergo HT, which in turn depends on the initial concentration of **1**. This is evident in the comparison of Figures S7 a and b, where the HT onset and the excited electron lifetime (and therefore the rate of ET) both exhibit saturation behavior similar to that seen for PL quenching (Figure S2). To estimate the HT and ET timescales at low **1** coverage, we consider the pre-saturation linear ranges in Figure S7a for HT and S7b (red) for ET. We do not have enough information to determine the number of molecules adsorbed per NR for each mixing ratio, but since the **1**:CdS NR ratio is <20 in the linear range, we can estimate that there are 1-10 adsorbed molecules per NR. The onset of ET, and therefore the timescale for HT is between 100 ps and 1 ns (Table S1 and Figure S7a). The range for τ_{ET} is 10-100 ns (Table S1).

Table S1. Results of analysis of TA dynamics displayed in Figure S6.

CdS NR:**1** ratio	Onset of ET (ps)	$<\tau_{measured}>$ (5-exp fit) (ns)	$<\tau_{measured}>$ (4-exp fit) (ns)	QE_{ET} (%)	$<\tau_{ET}>$ (ns)
1:0	N/A	160	Does not fit	N/A	N/A
1:8	370	44	43	72	61
1:12	250	11	11	92	12
1:19	130	4.3	3.9	96	4.5
1:60	115	3.4	3.0	97	3.5
1:94	90	1.0	1.0	99	1.0

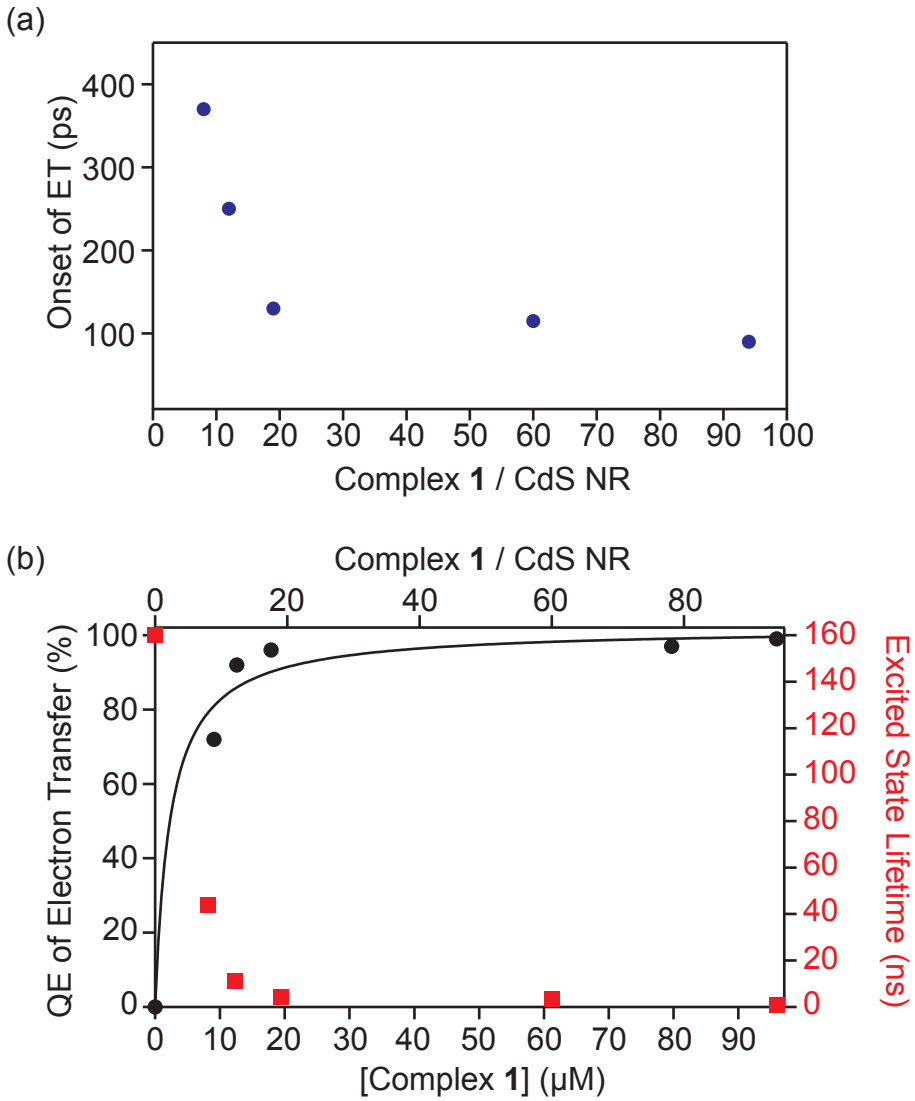

Figure S7. (a) The onset of ET as a function of **1**:CdS NR ratio. (b) QE_{ET} and the excited electron lifetimes plotted versus both concentration of **1** and **1**:CdS NR ratio. The three quantities plateau at high ratios. The QE_{ET} was fit with the Langmuir isotherm model (Eq. S3) and the resulting parameters were $K=4.2\times10^5$ M^{-1} and $(\Delta I/I_0)_{max} = 1.0$. The difference in the values of K seen in the PL and TA can be attributed to the difference in CdS NR concentrations between the two experiments.[13]

References

(1) Brown, K. A.; Wilker, M. B.; Boehm, M.; Dukovic, G.; King, P. W. *J. Am. Chem. Soc.* **2012**, *134*, 5627.
(2) Peng, P.; Sadtler, B.; Alivisatos, A. P.; Saykally, R. J. *J. Phys. Chem. C* **2010**, *114*, 5879.
(3) Robinson, R. D.; Sadtler, B.; Demchenko, D. O.; Erdonmez, C. K.; Wang, L. W.; Alivisatos, A. P. *Science* **2007**, *317*, 355.
(4) Tseng, H. W.; Zong, R.; Muckerman, J. T.; Thummel, R. *Inorg. Chem.* **2008**, *47*, 11763.
(5) Wasylenko, D. J.; Ganesamoorthy, C.; Koivisto, B. D.; Henderson, M. A.; Berlinguette, C. P. *Inorg. Chem.* **2010**, *49*, 2202.
(6) McDaniel, A. M.; Tseng, H. W.; Damrauer, N. H.; Shores, M. P. *Inorg. Chem.* **2010**, *49*, 7981.
(7) Brus, L. *Journal of Physical Chemistry* **1986**, *90*, 2555.
(8) Van de Walle, C. G.; Neugebauer, J. *Nature* **2003**, *423*, 626.
(9) *Semiconductors-Basic Data*; 2nd ed.; Madelung, O., Ed.; Springer: Berlin, 1996.
(10) Pavlishchuk, V. V.; Addison, A. W. *Inorg. Chim. Acta* **2000**, *298*, 97.
(11) Connelly, N. G.; Geiger, W. E. *Chem. Rev.* **1996**, *96*, 877.
(12) Klimov, V. I.; Schwarz, C. J.; McBranch, D. W.; Leatherdale, C. A.; Bawendi, M. G. *Phys. Rev. B* **1999**, *60*, R2177.
(13) Munro, A. M.; Jen-La Plante, I.; Ng, M. S.; Ginger, D. S. *J. Phys. Chem. C* **2007**, *111*, 6220.
(14) Klimov, V. I. *Annu. Rev. Phys. Chem.* **2007**, *58*, 635.
(15) Wu, K. F.; Zhu, H. M.; Liu, Z.; Rodriguez-Cordoba, W.; Lian, T. Q. *J. Am. Chem. Soc.* **2012**, *134*, 10337.
(16) Warren, J. J.; Mayer, J. M. *J. Am. Chem. Soc.* **2010**, *132*, 7784.
(17) Lakowicz, J. R. *Principles of Fluorescence Spectroscopy*; Springer: New York, 2006.